Wavelength-Resolved Oxime Ester Photoinitiator Decay in Radical Polymerization

Dushani Kanchana, Joshua A. Carroll, Nicolas Giacoletto, Didier Gigmes, Jisu Kim, Andreas N. Unterreiner, Kai Mundsinger,* Bryan T. Tuten,* and Christopher Barner-Kowollik*

ABSTRACT: We examine the wavelength-dependent efficiency of a set of oxime ester based photoinitiators via photopolymerization action plots in methyl methacrylate (MMA), assessing the polymer yield wavelength-by-wavelength after irradiation between 325 and 460 nm with a constant number of photons at each wavelength. We systematically vary the structural elements within three carbazole-based oxime esters, i.e., **1**, 1-(9-dodecyl-6-nitro-9*H*-carbazol-3-yl)-ethan-1-one *O*-acetyl oxime, **2**, 1-(9-dodecyl-6-nitro-9*H*-carbazol-3-yl)ethan-1-one *O*-(4-methoxybenzoyl) oxime, and **3**, 1-(9-dodecyl-6-nitro-9*H*-carbazol-3-yl)ethan-1-one *O*-(4-nitrobenzoyl) oxime, changing their substitution pattern on the carboxyl group from alkyl to two substituted aromatic functionalities. The resulting photopolymerization action plots are strongly mismatched with the extinction spectra of each oxime ester photoinitiator by close to 75 nm to the red edge of the main absorption maximum. The strongly red-shifted reactivity confirms that—at least under the examined conditions—extinction spectra constitute no valid guide for predicting maximum photopolymerization yields. We subsequently examine the wavelength-resolved dependence of the initiator decay in two solvents in the absence of MMA yet identical initiator concentrations by following the photofragmentation reaction via ^{1}H NMR spectroscopy. In both examined solvents, i.e., dimethyl sulfoxide (DMSO) and methyl isobutyrate (MIB), the obtained photoinitiator decay action plots also display a significant mismatch between the extinction spectrum and the wavelength-resolved photochemical action. The maximum reactivity in MIB and DMSO is red-shifted by close to 50 and 65 nm, respectively, and the photochemical action plot in DMSO exhibits a secondary local maximum. Notably, the decay action plots also do not display a reactivity maximum at the absorption maximum. We submit that the red-shifted maximum of the initiator decay is correlated with the enhanced photopolymerization activity on the red-edge of the absorption spectrum.

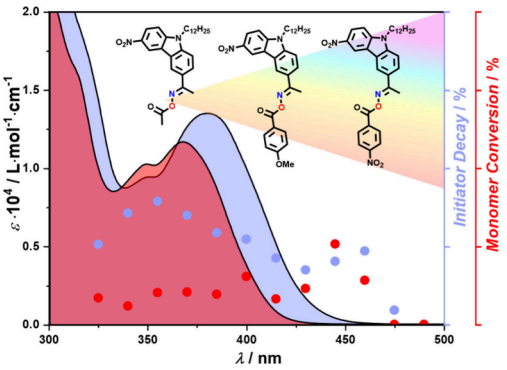

INTRODUCTION

Photochemistry is currently undergoing a shift toward the highly wavelength-resolved study of reaction outcomes underpinned by photochemical action plots.[1] In a photochemical action plot, the conversion of a starting material or yield of a photoproduct—or a set of photoproducts—is assessed after the reaction mixture has been exposed to a precisely defined number of photons at a specific wavelength emitted from an optical parametric oscillator (OPO), in the following referred to as a tunable laser.[2] Critically, wavelength-resolved data points from a photochemical action plot are obtained with an identical number of photons deposited into the reaction mixture at each monochromatic wavelength. Reliable data is obtained in the regime where the conversion is linearly correlated with the number of absorbed photons. The resulting photochemical action is graphed as a function of wavelength, typically in conjunction with the extinction spectrum of the reaction mixture. We note that in the following we will refer to extinction spectra as absorption spectra, noting that the difference is minimal given that scattering effects are minimal at low substrate concentrations. While the technique has proven to be a powerful tool for outcome-based investigations of photoreactions, it does not provide insight into the underlying photophysical processes that lead to the observed outcomes. Initially, the photochemical action plot technique has been applied to photopolymerization reactions, specifically the free-radical polymerization of methyl methacrylate (MMA) initiated by two oxime ester-based photoinitiators, i.e., *O*-benzoyl-*α*-oxooxime, **OXE01**, and *O*-acetyloxime, **OXE02**.[3] Surprisingly—at the time and perhaps still today—we found that there exists a pronounced mismatch between the absorption spectrum of the photoinitiator and MMA reaction mixture and the photochemical action under the examined

Scheme 1. Chemical Structures of the Three Examined Oxime Ester Based Photoinitiators 1-(9-Dodecyl-6-nitro-9*H*-carbazol-3-yl)ethan-1-one *O*-acetyl Oxime 1, 1-(9-Dodecyl-6-nitro-9*H*-carbazol-3-yl)ethan-1-one *O*-(4-Methoxybenzoyl) Oxime 2, and 1-(9-Dodecyl-6-nitro-9*H*-carbazol-3-yl)ethan-1-one *O*-(4-Nitrobenzoyl) Oxime 3) as Well as the Two Previously Investigated Initiators (*O*-Benzoyl-*α*-oxooxime OXE01 and *O*-Acetyloxime OXE02) alongside the General Fragmentation Mechanism of Oxime Ester Photoinitiators[a]

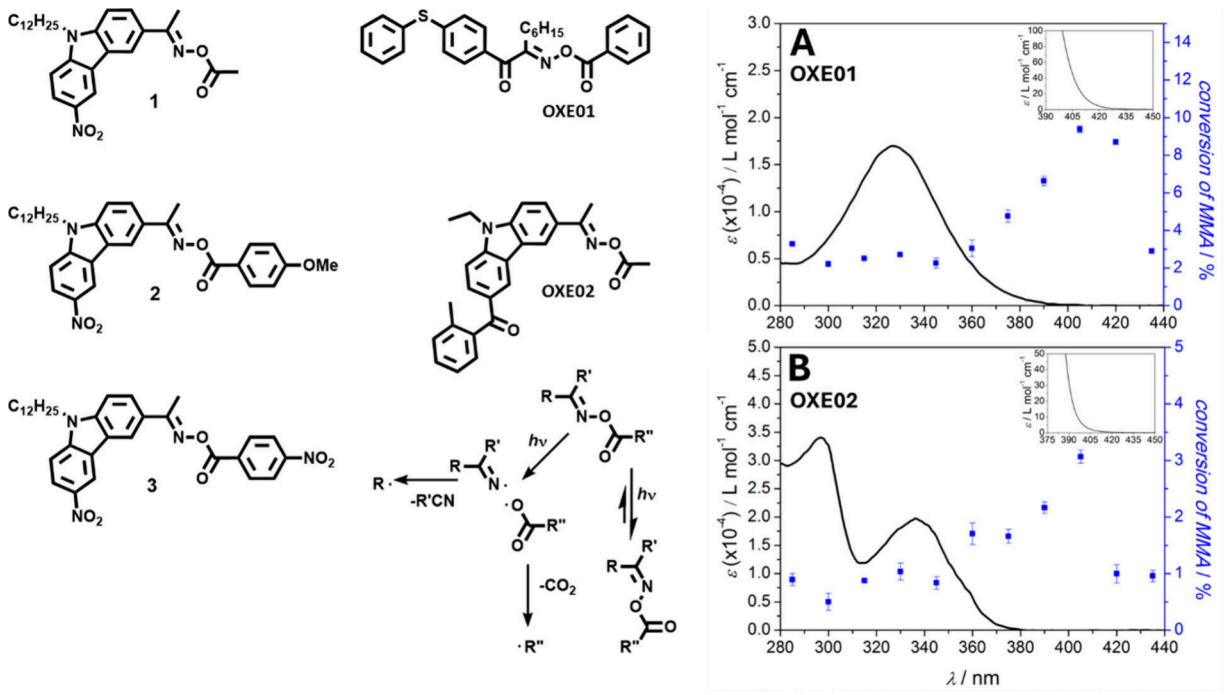

[a]The right-hand panel displays the photochemical action plots of **OXE01** (A) and **OXE02** (B) reported in 2017.[3]

reaction conditions, demonstrating that peak reactivity as assessed by monomer-to-polymer conversion was reached at extremely low molar extinctions to the red-side of the absorption spectrum. Our initial study carefully assessed the product spectrum generated via high resolution mass spectrometry in terms of the polymer end groups and found only limited wavelength variance.[3]

Interestingly, in the meantime, strong photopolymerization activities—including maximum polymerization activities—have been observed by other groups at extremely low absorptivities. For example, most recently the teams of Junkers and Perrier reported that the most rapid polymerization rates for a range of photoinduced reversible addition−fragmentation chain transfer (RAFT) polymerizations were obtained under conditions where the absorbances of the RAFT agents were very small,[4] not dissimilar to results obtained by Konkolewicz and colleagues in an earlier study on the photopolymerization of vinyl ketones, who found that maximum rates are obtained well on the red-edge of the absorption spectrum of the reaction mixture.[5] In a further example, Haddleton and colleagues observed remarkably rapid polymerization activities in photo-induced atom transfer radical polymerization (ATRP) at very low absorptivities well beyond the main absorption region of the reaction mixture.[6] While these and similar studies certainly do not contain photochemical action plots that adhere to their stringent conditions such as identical photon count at each wavelength, conversion in the linear reaction kinetic regime and no more than 50% absorption at each wavelength,[2] they do point to the widespread nature[7] of the effect we discovered in 2017.[3] It is important to note that the cause of disparate photochemical action plots with absorbance spectra is complex and highly system specific.[8] It may entail complex excited state dynamics and environmental effects—such as the relative permittivity of the solvent—as well as complex reaction kinetics caused by emerging product species and their absorbance spectra.

Over the past decade, our attention has largely focused on examining the wavelength-resolved behavior of small molecule reactions—where we identified a similar absorptivity/reactivity mismatch[2,9−14] for a large number of reaction systems—given the inherently complex nature of photopolymerization systems. We now return to photopolymerization systems, as our initial study is to date the only one investigating the wavelength dependence of oxime ester initiated photopolymerization via a valid action plot. We submit that it is critical to assess a more expansive set of oxime ester based photoinitiators via photochemical action plots to establish if the initially observed phenomena hold true for a wider set of oxime initiators, given the interest in this important class of photoinitiators.[15,16] Critically, herein, we aim to investigate and isolate the initiator-decay action plot from the photopolymerization action plots via photochemical action plots of the initiator decay in a nonpolymerizing environment that, however, mimics the monomer in terms of polarity and viscosity as closely as possible.

Scheme 1 depicts an overview of the examined photo-initiators alongside the photoinitiators and their respective photochemical action plots that we have examined in our earlier study.[3] We systematically vary the structure of the photoinitiators: whereas our initial study examined a structural variation on both sides of the oxime ester functionality, we now

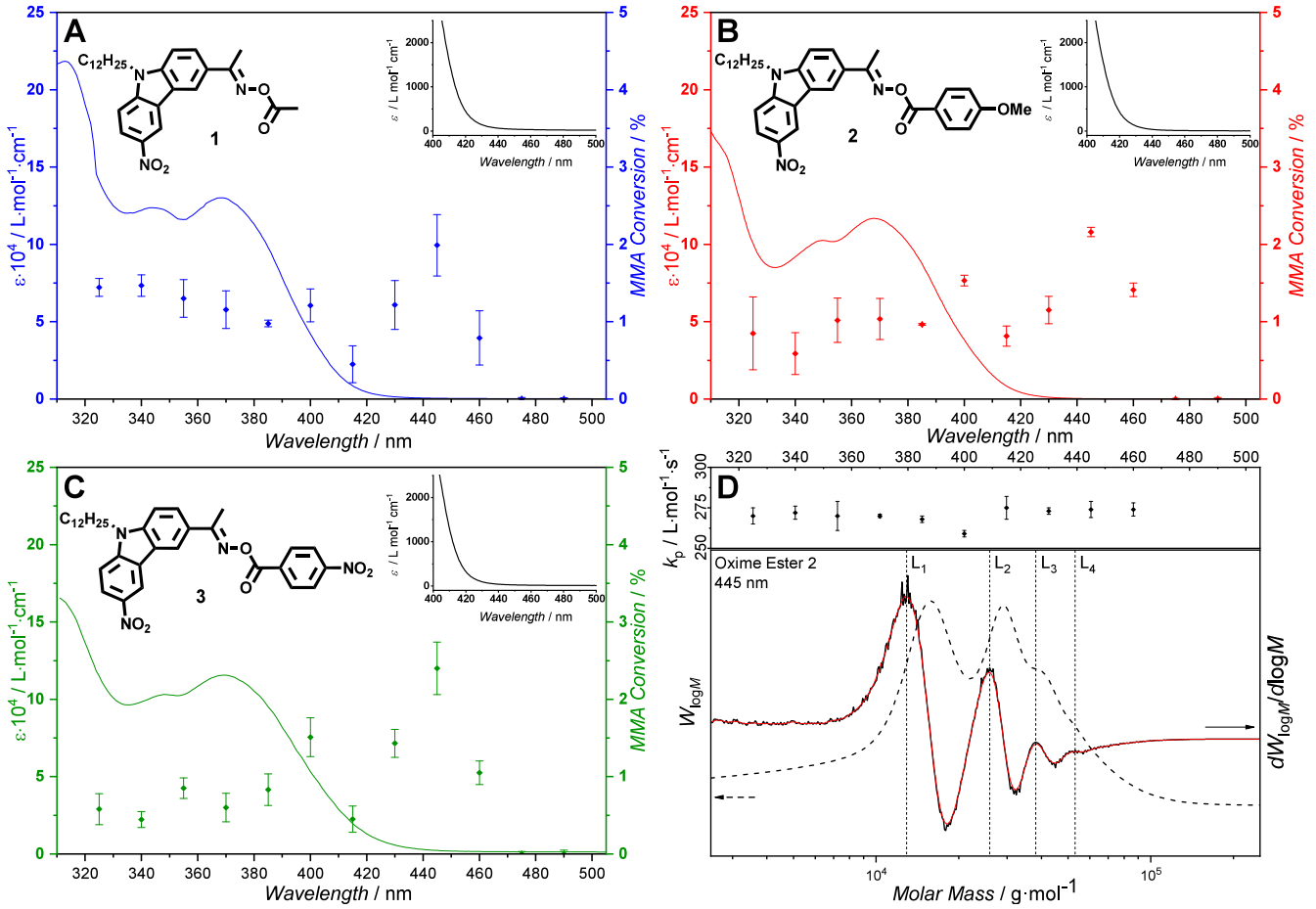

Figure 1. Photopolymerization action plots in bulk methyl methacrylate (MMA) at ambient temperature of oxime ester **1** in (A), oxime ester **2** in (B), and oxime ester **3** in (C) as well as the corresponding extinction spectrum of each oxime ester. The oxime ester concentration was 5×10^{-3} mol L^{-1} in each case, and 3.67×10^{19} photons were deposited at each monochromatic wavelength. The entire data set is available in Supporting Information Section 2.3. (D) Propagation rate coefficient k_p at each wavelength for the polymerizations using oxime ester **2** (at 475 and 490 nm no polymer was obtained) at ambient temperature. The lower panel D depicts an exemplary molar mass distribution obtained after irradiation (dashed line) and its first derivative (black line) smoothed (red line) to determine the inflection points L_i for the determination of the propagation coefficient, k_p. Refer to Supporting Information Section 4.1 for the analysis of the molar mass distribution as well as further obtained distributions at different wavelengths.

kept the substituent at the N-terminus constant, while varying the O-terminus substitution as depicted.

EXPERIMENTAL SECTION

Materials. 1-(9-Dodecyl-6-nitro-9*H*-carbazol-3-yl)ethan-1-one *O*-acetyl oxime (Oxime Ester 1), 1-(9-dodecyl-6-nitro-9*H*-carbazol-3-yl)ethan-1-one *O*-(4-methoxybenzoyl) oxime (Oxime Ester 2), and 1-(9-dodecyl-6-nitro-9*H*-carbazol-3-yl)ethan-1-one *O*-(4-nitrobenzoyl) oxime (Oxime Ester 3) were kindly provided by the group of Gigmes at the ICR, Aix Marseille University, France.[17] Methyl methacrylate (MMA, Sigma-Aldrich, 99%, stabilized) was freed from inhibitor by passing through a column of activated basic alumina (Sigma-Aldrich). Deuterated dimethyl sulfoxide (DMSO-d_6, Novachem, 99.9 atom % D), deuterated chloroform ($CDCl_3$, Novachem, 99.8 atom % D), and methyl isobutyrate (MIB, Merck, 99%) were used as received.

UV–Vis Spectroscopy. UV–vis spectra were recorded on a Shimadzu UV-2700 PC UV–vis scanning spectrophotometer in MMA, MIB, and DMSO-d_6. Molar extinction coefficients (ε) were determined over a range ($A_{\lambda_{max}} < 1$) of at least three concentrations, the resulting absorbance spectra normalized by their molar concentration and subsequently averaged. To resolve the absorbance tail ($\lambda > 400$ nm) solutions of higher concentrations (>1 absorbance at λ_{max}) were used.

Variable Wavelength Pulsed Laser Polymerization (PLP) and Photoinitiator Decay. For PLP the samples were all prepared with a concentration of $c_{photoinitiator} = 5 \times 10^{-3}$ mol L^{-1} in MMA (sample volume ~0.5 mL) and freed from oxygen by purging with nitrogen for 5 min. Subsequently, the samples were individually placed into the sample holder and irradiated at ambient temperature. The polymerization was induced by a tunable Opotek Opolette HE 355 LD laser system with a 5 ns pulse duration, 20 Hz pulse repetition rate, and a constant photon count at each wavelength (refer to Supporting Information, Section 2.2, for a detailed description of the calibration procedure). After the polymerization, the remaining monomer was evaporated, and the polymer was analyzed without any purification. Monomer conversions were determined gravimetrically (refer to Supporting Information, Section 2.3).

For the photoinitiator decay studies, all samples were prepared with a concentration of $c_{photoinitiator} = 5 \times 10^{-3}$ mol L^{-1} in MIB and DMSO-d_6 (sample volume 0.5 mL). Subsequently, the samples were individually placed into the sample holder and irradiated at ambient temperature. The irradiation was carried out analogous to the procedure described above. After the irradiation ^{1}H NMR spectra were recorded for each sample. For samples in MIB the solvent was evaporated in the dark and the solid residue was dissolved in DMSO-d_6, prior to ^{1}H NMR analysis).

High-Resolution SEC-ESI-MS. SEC-MS measurements were performed on a Dionex UltiMate 3000 UHPLC system consisting

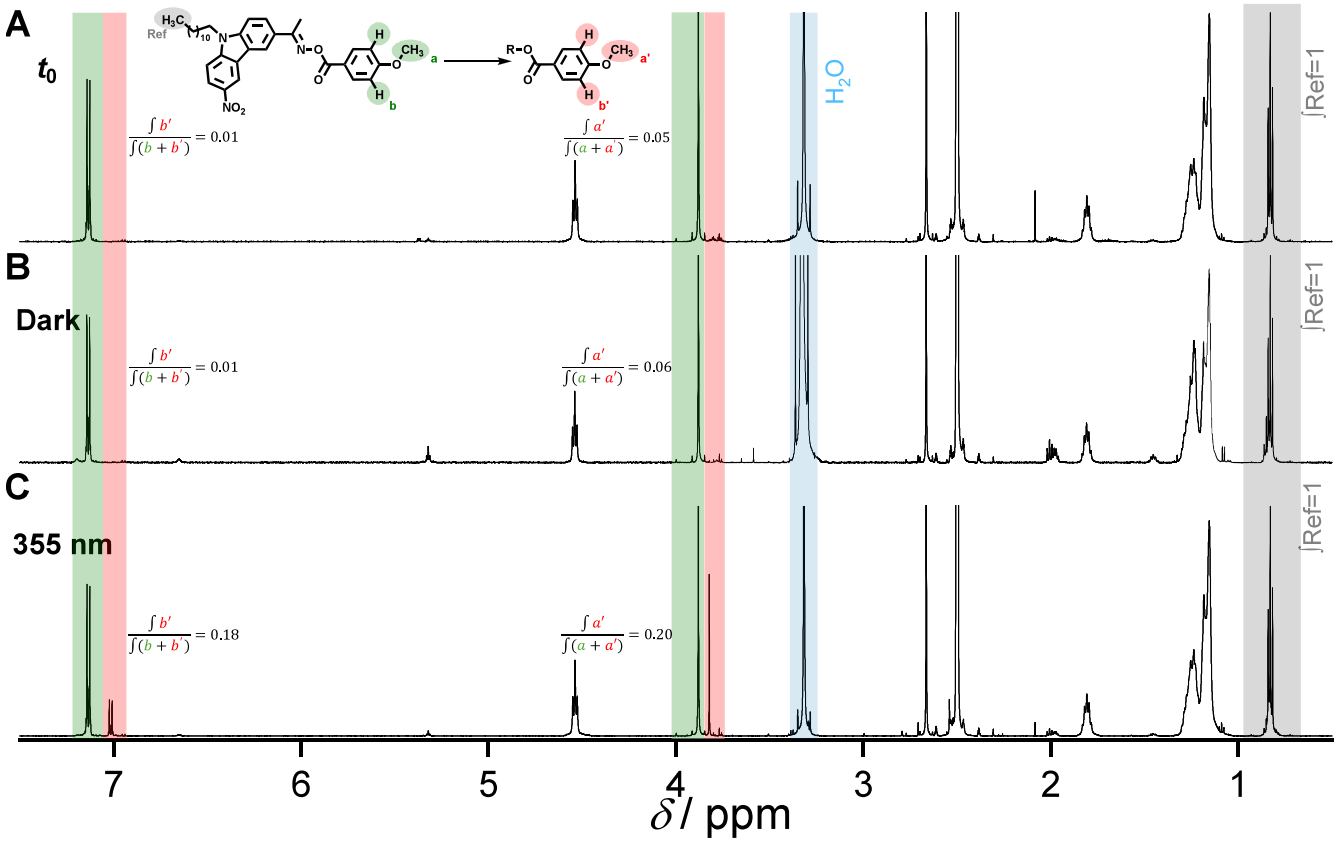

Figure 2. Exemplary ^{1}H NMR spectra of oxime ester **2** (1-(9-dodecyl-6-nitro-9*H*-carbazol-3-yl) ethan-1-one *O*-(4-methoxybenzoyl) oxime) recorded in DMSO-d_6 ($c = 5 \times 10^{-3}$ mol L^{-1}). (A) depicts the ^{1}H NMR spectrum before laser irradiation, (B) the ^{1}H NMR spectrum of a reaction mixture that was not irradiated but otherwise carried through the experimental procedure, while (C) depicts the ^{1}H NMR spectrum of oxime ester **2** after irradiation with 7.86×10^{18} photons at 355 nm. Resonances used for quantification are depicted in colored highlights: resonances related to intact oxime ester **2** in green, resonances of daughter species **2′** in red, resonances used as internal standard in gray. Refer to Supporting Information Section 4.2 for all recorded and evaluated ^{1}H NMR spectra.

of a pump (LPG 3400SD), autosampler (WPS 3000TSL), and column oven (TCC 3000). The pump and autosampler were modified for use with THF. Polymers were dissolved at 2 mg/mL in THF, and a 100 μL aliquot was injected onto three consecutive mixed bead size exclusion chromatography columns (PSS, SDV micro columns 3 μm 1000 Å 4.6 × 250 mm) with a precolumn (SDV micro precolumn 3 μm 4.6 × 30 mm), maintained at 30 °C. THF was used as the eluent at a flow rate of 0.3 mL/min. The post-column eluate was split 9:1 (v/v) and the larger fraction was analysed by a UV detector (VWD 3400, Dionex) and an RI-detector (RefractoMax520, ERC, Japan) in a setup described earlier.[18] The remaining 10% was combined with a sodium iodide solution (50 μM in methanol), infused at 20 μL/min by a micro-flow HPLC syringe pump (Teledyne ISCO 100DM). The combined solution was directed into the heated electrospray ionisation source of a Q Exactive Plus Biopharma high-resolution Orbitrap mass spectrometer (Thermo Fisher Scientific, Bremen, Germany). The instrument was calibrated using ammonium hexafluorophosphate over the m/z range 600−8000. The spray voltage was set to 3.5 kV, and the sheath and auxiliary gas (N2) flow rates were set to 10 and 0 (dimensionless arbitrary units), respectively. The capillary temperature was set to 320 °C, the S-lens RF level was set to 150, and the auxiliary gas heater temperature was set to 125 °C. Spectra were acquired at a nominal mass resolving power of 140,000 (defined at m/z 200). MSPolyCalc was used to simulate polymer spectra and compare to the experimental spectra.[19]

THF-SEC. The SEC measurements were conducted on a PSS SECurity2 system consisting of a PSS SECurity Degasser, PSS SECurity TCC6000 Column Oven (35 °C), *PSS* SDV Column Set (8 × 150 mm^2 5 μm Precolumn, 8 × 300 mm^2 5 μm Analytical Columns, 100000, 1000, and 100 Å) and an Agilent 1260 Infinity isocratic pump, Agilent 1260 Infinity standard autosampler, Agilent 1260 Infinity diode array and multiple wavelength detector (A: 254 nm; B: 360 nm), Agilent 1260 Infinity refractive index detector (35 °C). HPLC grade THF, stabilized with BHT, is used as eluent at a flow rate of 1 mL min^{-1}. Narrow disperse linear poly(methyl methacrylate) (M_n 202 to 2.2 × 10^6 g mol^{-1}) standards (PSS ReadyCal) were used as calibrants. All samples were passed over 0.22 μm PTFE membrane filters. Molar mass and dispersity analyses were performed in PSS WinGPC UniChrom software (version 8.33).

RESULTS AND DISCUSSION Photopolymerization

Action Plots of Oxime Photo-initiators.

We systematically investigate how the wavelength, via monochromatic irradiation, affects the photopolymerization yields initiated by oxime esters **1**, **2**, and **3** by recording the MMA to poly(methyl methacrylate) (PMMA) conversion between 325 and 490 nm at a constant photon count of 3.67×10^{19} photons at each monochromatic wavelength. The photopolymerization action plots of polymerizations initiated by **1**, **2**, and **3** suggest that the newly investigated oxime esters behave very similar to the already investigated two oxime initiators, demonstrating a strong red-shift of the polymerization efficiency compared to the absorbance spectrum. While the polymerization activity is relatively constant—at a low level—in regions where the absorptivity of the oxime esters is strongest, maximum activity occurs in regions of low absorptivity. Oxime ester **1** (λ_{max} = 368 nm) has its maximum polymerization yield at 445 nm (Δ = 77 nm), oxime ester **2**

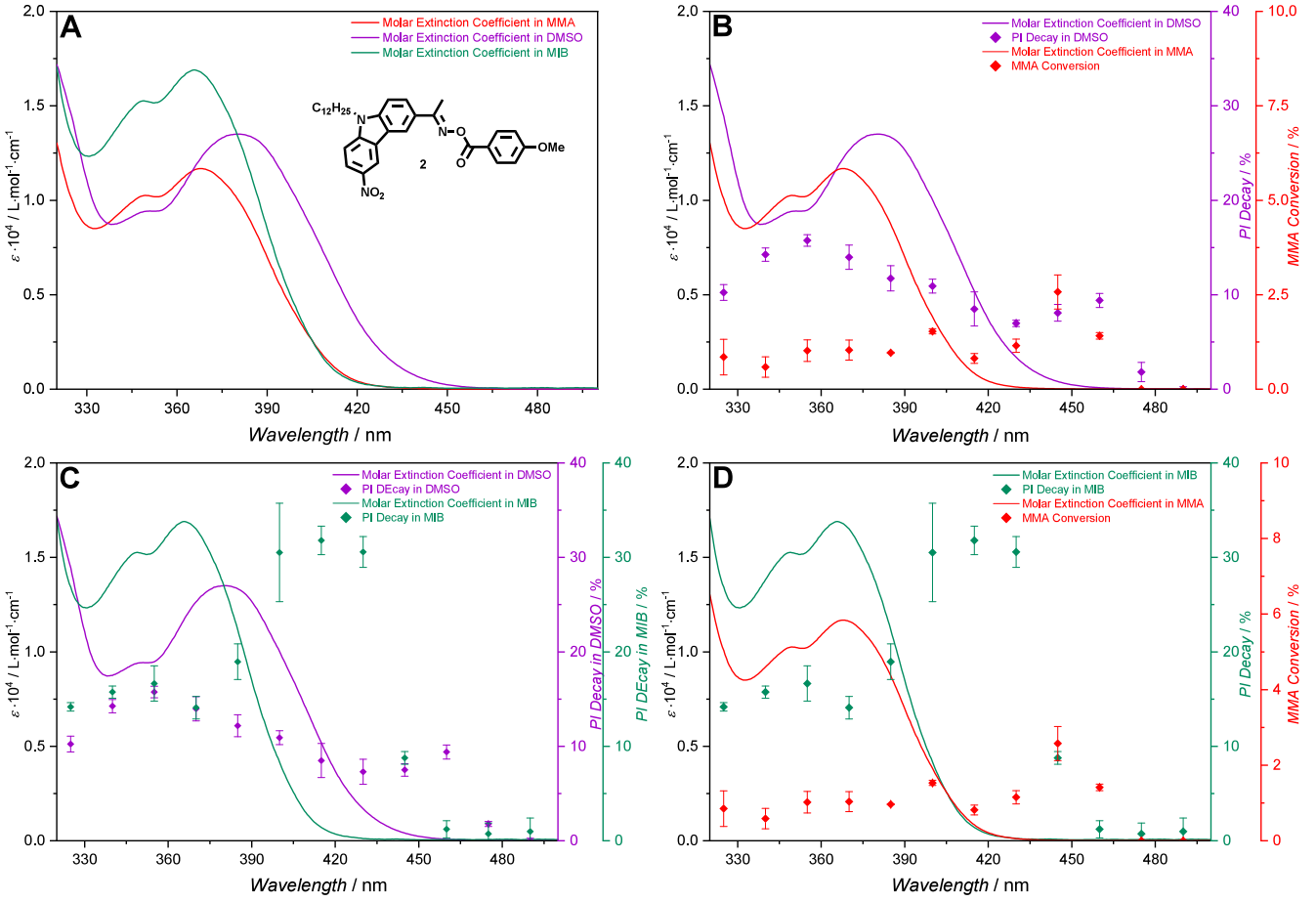

Figure 3. (A) Absorption spectra of oxime ester **2** in MMA (red) in DMSO-d_6 (purple) and in methyl isobutyrate (MIB) (green). Photochemical action plots of oxime ester **2** in (B) DMSO-d_6 (purple) and (D) (MIB) (green) alongside the absorption spectra of oxime ester **2** in the respective solvent at a concentration of 5×10^{-3} mol L^{-1}. (C) Overlay of oxime ester **2** decay action plots in two different solvents, DMSO-d_6 (purple) and MIB (green).

(λ_{max} = 368 nm) has its maximum polymerization yield at 445 nm (Δ = 77 nm), and oxime ester **3** (λ_{max} = 368 nm) has its maximum polymerization yield at 445 nm (Δ = 77 nm). The similarity of these values is not necessarily surprising as the carbazole motif is identical in all three initiators and largely responsible for their absorbance >350 nm. It is instructive to note that we observe—for all initiators—a local minimum in reactivity on the red-flank of the absorption spectrum. These encompassing observations for a total of five oxime ester photoinitiators may suggest that the entire initiator class behaves in a similar fashion in their response to polymerization activity at different wavelengths. All five initiators exhibit extinction maxima between 360 and 370 nm, however their maximum polymerization efficiency is red-shifted by approximately 75 nm (refer to Figure 1).

Before progressing to the examination of the initiator decay in isolation from the polymerization activity, we examined if the employed wavelengths had a notable effect on the polymerization reaction kinetics. Conveniently, the photochemical action plot experiments yield not only the monomer to polymer conversion at each wavelength, but also the full molar mass distribution for each wavelength and each initiator. We employed the generated molar mass data to deduce the free-radical polymerization propagation rate coefficient for each wavelength using the IUPAC recommended methodology for deducing propagation rate coefficients, k_p.[20−23] We determined the propagation rate coefficient at every examined wavelength for oxime ester **2** (refer to Figure 1D), and for oxime ester **1** and **3** at one short (325 nm) and one longer (445 nm) wavelength (refer to Supporting Information Section 4.1 for details) and found them to be well-aligned with literature values.[22] We determined an average k_p of 268 ± 8 L mol^{-1} s^{-1} at ambient temperature across all wavelengths and initiators, while the recommended IUPAC value reads 267 L mol^{-1} s^{-1} at 20 °C with an estimated uncertainty of 10%.[22] Not only do these data constitute the perhaps first fully wavelength dependent determination of the propagation rate coefficient of MMA at ambient temperature, but—in the context of the current study—suggest that the polymerization mechanism itself is not affected by the wavelength of the incident light.

Photodecay Action Plots of Oxime Photoinitiators. We subsequently selected one of the photoinitiators—oxime ester **2**—to investigate the photoreaction, i.e., the scission of the N−O bond, separately from the (photo)polymerization process. The photopolymerization effectively acts as a quantum yield amplifier for the initiator decay via the generated primary and secondary initiating radical species yet is itself subject to a complex set of reaction kinetics, i.e., the initiation, propagation and termination rate law equations, which constitute a system of coupled differential equations. Thus, examining the initiator decay in isolation is a critically important exercise. Since it is

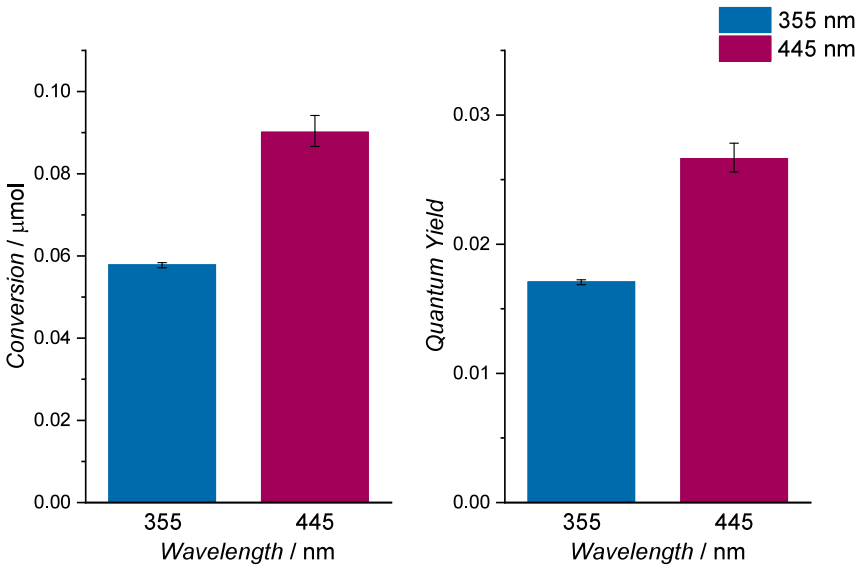

Figure 4. Conversion and quantum yield of oxime ester **2** at 355 and 445 nm in DMSO-d_6 using a solution where the concentration was adjusted to achieve identical absorbance at 355 nm (blue) and 445 nm (red). Absolute conversion is shown in μmol. All samples were irradiated with 2.04×10^{18} photons (3.4 μmol of photons).

highly challenging to isolate the initiator decay from the polymerization activity in a polymerizing medium such as MMA, we decided to replace MMA with suitable solvents. The closest structural analogue to MMA that does not undergo polymerization is methyl isobutyrate (MIB), as it resembles MMA with a hydrogenated double bond. The other solvent of choice is dimethyl sulfoxide (DMSO) as it solubilizes the oxime esters well and is readily available in its deuterated form, enabling facile tracking of the depletion of **2** via two of its diagnostic ^{1}H NMR resonances (labeled **a** and **b**) as depicted in Figure 2. It was possible to conduct the entire photochemical decay action plot in DMSO-d_6 and directly analyze the resulting reaction mixture via ^{1}H NMR spectroscopy. When conducting the photochemical action plot in MIB, the solvent had to be evaporated and the residue subsequently dissolved in a ^{1}H NMR suitable solvent for the determination of the fraction of decayed **2**. As we also conducted experiments in DMSO-d_6, we selected DMSO-d_6 to dissolve the residue from the MIB experiments. As depicted in Figure 2, the photoinitiator decay can be followed by tracking the disappearance of specific resonances at 7.1 ppm (**b**, $CH_{aromatic}$) and 3.9 ppm (**a**, $O-CH_3$) associated with the intact oxime ester, while concomitant resonances of emerging daughter species can be traced at 7.0 ppm (b′, $CH_{aromatic}$) and 3.8 ppm (a′, $O-CH_3$). A detailed description of the experimental procedure can be found in Supporting Information Section 2.4.

The results of the photoinitiator decay action plots are depicted in Figure 3, graphed for comparison with the photopolymerization action plots discussed above. A comparison of the initiator decay of **2** in MIB and DMSO reveals the specificity of the action plot methodology toward the investigated system. The solvatochromatic shift of λ_{max} indicates the relative permittivity[24] of the investigated systems and highlights that MIB is slightly less polar than MMA while DMSO is significantly more polar. This ranking was further underpinned by investigation of the solvatochromism of the literature known dye Eosin Y in the investigated solvents (refer to Supporting Information Section 2.1). Here, the shift of the lowest energy absorbance band of Eosin Y in each solvent follows the same trend as the absorbance observed for oxime ester **2**, with the same solvent dependence also observed in the photoinitiator decay profiles. For the photoinitiator decay action plot in MIB, we observed a local maximum decay at 415 nm, red-shifted by approximately 50 nm from the absorbance maximum in MIB. In DMSO, however, the action plot exhibits two local maxima at 355 and 460 nm, while the absorbance maximum is close to 380 nm. The local maximum at 460 nm is at a similar wavelength to what we observed in the polymerization action plots, however, the overall decay maximum is close to 355 nm. At first glance this seems to be a blue shift from the absorbance maximum. We propose, however, that this reactivity maximum is red-shifted from an absorbance band hidden in the UV cutoff of DMSO. Overall, the initiator decay action plots suggest that the enhanced photopolymerization activity on the red side of the absorption spectrum is mirrored in the initiator decay action plots. We note, however, that neither solvent perfectly mimics the environment that MMA constitutes and thus the photopolymerization and photodecay action plot maxima to the red side of the absorption spectrum are not expected to fully coincide. Nevertheless, we submit that the wavelength-resolved decay of the photoinitiator is qualitatively mirrored in the photopolymerizations.

To further examine the reactivity enhancement of the photoinitiator on the red side of the absorption spectrum, we subsequently investigate the photoinitiator decay at two wavelengths by adjusting their concentration to achieve an identical absorbance at each wavelength. In such a scenario, the number of photons absorbed by the initiator is identical at each excitation wavelength. If the data in the photochemical decay action plot are valid, one would expect a more pronounced decay at the red-edge maximum decay activity wavelength, than at a more blue-shifted position, as this experiment effectively mirrors the quantum efficiency of the system, i.e., conversion obtained for an identical number of *absorbed* photons. To test this hypothesis, 355 and 445 nm were selected as excitation wavelengths, as we observed two distinct local maxima of photoinitiator decay at these regions

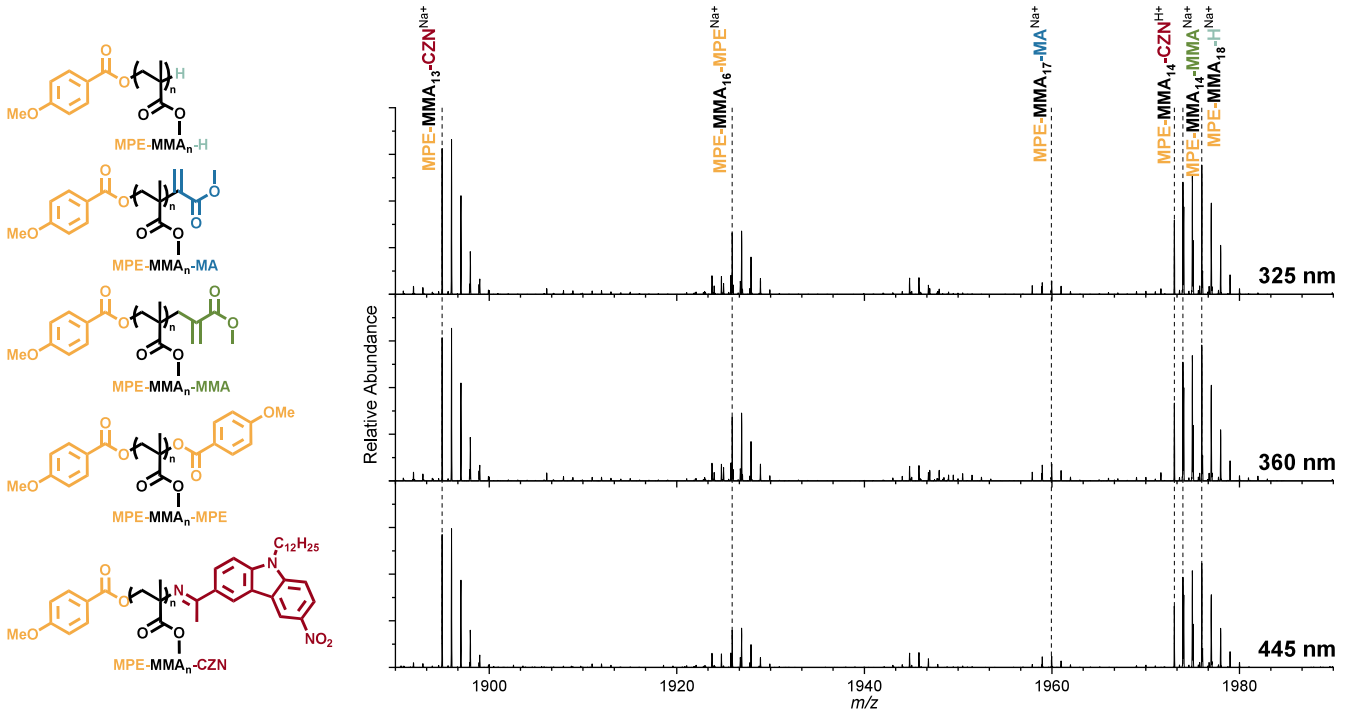

Figure 5. Structures of end groups identified via mass spectrometry of polymers obtained by polymerizing methyl methacrylate (MMA) with oxime ester **2** on the left. Zoom into one representative repeat unit of size exclusion chromatography hyphenated mass spectra (SEC-ESI-MS) of polymers that were irradiated at 325 nm, 360 and 445 nm. Spectra were extracted from the peak eluting at 25–26 min, corresponding to 5000 g mol^{-1} to 20000 g mol^{-1}. Refer to Supporting Information Section 4.3 for the full mass spectra as well as the simulated isotopic patterns of the identified ions in comparison with the experimentally observed peak patterns for each ion.

when **2** was irradiated in DMSO-d_6. The solutions exhibited an absorbance of 3.22, implying less than 0.1% of the incident photons were transmitted through the sample. Figure 4 confirms the above notion, that 445 nm is the more effective wavelength in inducting initiator decay with a measured quantum yield of 0.027, while the quantum yield measured at 355 nm was only 0.017 (a ratio of 1.56).

To investigate the difference in polymerization efficiency at different wavelengths, we conducted SEC-electrospray ionization mass spectrometry (ESI-MS) analysis of the polymers that were generated with oxime ester **2** at 325, 360, and 445 nm (refer to Figure 5). The aim of the mass spectrometric analysis is to determine if the generated end group pattern is invariant to the employed wavelength. Changes in end group pattern with wavelength may suggest a change in the type of radicals generated as a function of wavelength, potentially contributing to the observed wavelength-dependent photopolymerization behavior. However, as inspection of Figure 5 indicates, we observed minimal differences in the relative intensities of the ions representing polymer chains with end groups we were able to identify. Note that Figure 5 displays one representative repeat unit, with the other repeat units displaying a very similar ion pattern. The high-resolution mass spectra also suggest the presence of one signal set between 1940 and 1950 m/z that cannot be assigned to a known end group combination of initiating radical fragments. However, this signal set is present at every examined wavelength and thus does not indicate a wavelength dependent reaction channel. We note that the SEC-ESI-MS technique—where polymer chains are preseparated prior to high solution mass spectrometric analysis—is restricted to the smaller size end of the molar mass distributions due to the restriction in ionization ability of the ESI process. However, ESI remains the only viable analytical option, as matrix assisted laser desorption and ionization (MALDI) mass spectrometry is a light-driven method, with a strong likelihood of altering the end groups of the polymer chains, which may retain their ability to photofragment, especially under the typically high laser intensities used during MALDI-MS.[25]

CONCLUSIONS

We examine three oxime ester type photoinitiators in their ability to effect photopolymerization of methyl methacrylate (MMA) as a function of wavelength, using our photochemical action plot methodology. We demonstrate that all three initiators **1**, **2**, and **3** show a similar behavior in terms of their wavelength-dependent reactivity, suggesting a strong red-shift of their polymerization activity compared to the absorption maximum of the employed oxime photoinitiator. Our data suggest that the class of oxime initiators—at least on the basis of the thus far examined five initiators (**OXE01**, **OXE02** (previous study) and oxime esters **1**, **2**, and **3** (current study))—show common behavior with regard to the observed, red-shifted activity with an average red-shift of 75 ± 7.5 nm (uncertainty estimated based on the 15 nm sampling resolution). On this basis, we recommend that oxime esters show their best performance to the red-side of the absorption maximum and should be activated in the associated wavelength regime. Therefore, a wavelength-resolved investigation of their activity is critical for the development of advanced photopolymerization systems. This is essential to achieve faster manufacturing speeds by leveraging the synergy between deeper penetration at longer wavelengths and the higher reactivity of the initiating compounds. Based on our

observations, we recommend an initiation wavelength red-shifted by approximately 75 nm from the maximum absorbance wavelength of the specific oxime ester, as this shift has consistently been observed with oxime esters with various substituents. We have observed similarly red-shifted behavior, by 80 nm, in photopolymerizations initiated by BAPO-type photoinitiators,[26] suggesting that—similar to small molecule photochemical processes—the mismatched behavior of photopolymerization activity and absorptivity of the reaction system may be prevalent in many photopolymerization reactions.

Critically, we unpack for one of our investigated initiators the initiator decay as a function of wavelength in two nonpolymerizing solvents: DMSO and MIB. We find that in both solvents a secondary red-shifted absorption maximum can be observed, which is in its position solvent dependent. We thus submit that the enhanced polymerization activity at red-shifted wavelengths is caused—at least in part—by an enhanced generation of primary radicals on the red-side of the absorption spectrum of the photoinitiator. In an experiment probing the initiator decay as a function of absorbed photons, we demonstrate that the quantum yield for the photocleavage of oxime ester **2** is considerably higher at 445 nm (0.027) than determined at 355 nm (0.017), by a factor of 1.56. With no difference observed in the end groups of the resulting polymer, we further submit that the cause of the red-shifted reactivity is likely associated with a wavelength dependent intermediate process between the photoexcitation and the radical polymerization. Sameshima et al. reported that for similar oxime esters, the N–O bond photocleavage from the triplet state led to reduced radical recombination, and thus more effective diffusional dissociation into free radicals than for photocleavage from the singlet state.[27] We submit that the proportion of triplet cleavage to singlet cleavage for our oxime esters is possibly wavelength dependent, with longer wavelength excitations providing more effective access to the triplet state, and thus more free radical diffusion, rather than a change in the type of primary radicals that are generated. We base this interpretation on the observation that the end group pattern of the generated polymers is invariant to wavelength, with exactly the same initiating species found at each examined wavelength. As a concluding remark we highlight the necessity to expand the substrate scope of wavelength resolved reactivity studies and the investigation of the underlying photophysical processes.

AUTHOR INFORMATION

Corresponding Authors

Kai Mundsinger – *School of Chemistry and Physics, Centre for Materials Science, Queensland University of Technology (QUT), Brisbane, QLD 4000, Australia*; Email: k.mundsinger@qut.edu.au

Christopher Barner-Kowollik – *School of Chemistry and Physics, Centre for Materials Science, Queensland University of Technology (QUT), Brisbane, QLD 4000, Australia; Institute of Nanotechnology (INT), Karlsruhe Institute of Technology (KIT), 76344 Eggenstein-Leopoldshafen, Germany*; orcid.org/0000-0002-6745-0570; Email: christopher.barnerkowollik@qut.edu.au, christopher.barner-kowollik@kit.edu

Bryan T. Tuten – *School of Chemistry and Physics, Centre for Materials Science, Queensland University of Technology (QUT), Brisbane, QLD 4000, Australia; Department of Chemistry and Biochemistry, The University of Texas at Tyler, Tyler, Texas 75799, United States*; orcid.org/0000-0002-5419-7561; Email: bryan.tuten@qut.edu.au

Authors

Dushani Kanchana – *School of Chemistry and Physics, Centre for Materials Science, Queensland University of Technology (QUT), Brisbane, QLD 4000, Australia*

Joshua A. Carroll – *School of Chemistry and Physics, Centre for Materials Science, Queensland University of Technology (QUT), Brisbane, QLD 4000, Australia*

Nicolas Giacoletto – *CNRS, ICR UMR 7273, Aix Marseille Univ, F-13397 Marseille, France*

Didier Gigmes – *CNRS, ICR UMR 7273, Aix Marseille Univ, F-13397 Marseille, France*

Jisu Kim – *School of Chemistry and Physics, Centre for Materials Science, Queensland University of Technology (QUT), Brisbane, QLD 4000, Australia; Institute of Physical Chemistry (IPC), Karlsruhe Institute of Technology (KIT), 76131 Karlsruhe, Germany*

Andreas N. Unterreiner – *Institute of Physical Chemistry (IPC), Karlsruhe Institute of Technology (KIT), 76131 Karlsruhe, Germany*; orcid.org/0000-0002-1225-5460

Notes

The authors declare no competing financial interest.

ACKNOWLEDGMENTS

C.B.-K. and B.T. acknowledge funding for the current project in the context of an Australian Research Council (ARC) Linkage grant in collaboration with MicroTau Pty. Ltd. D.K. is grateful for a PhD scholarship form the Queensland University of Technology (QUT). The Central Analytical Research Facility (CARF) at QUT is gratefully acknowledged. J.K. thanks the Karlsruhe Institute of Technology (KIT) for a PhD scholarship.

REFERENCES

(1) Roth, H. D. The beginnings of organic photochemistry. *Angew. Chem. Int. Ed.* **1989**, *28* (9), 1193–1207.

(2) Irshadeen, I. M.; Walden, S. L.; Wegener, M.; Truong, V. X.; Frisch, H.; Blinco, J. P.; Barner-Kowollik, C. Action Plots in Action: In-Depth Insights into Photochemical Reactivity. *J. Am. Chem. Soc.* **2021**, *143* (50), 21113–21126.

(3) Fast, D. E.; Lauer, A.; Menzel, J. P.; Kelterer, A.-M.; Gescheidt, G.; Barner-Kowollik, C. Wavelength-Dependent Photochemistry of Oxime Ester Photoinitiators. *Macromolecules* **2017**, *50* (5), 1815–1823.

(4) Bereś, M. A.; Zhang, B.; Junkers, T.; Perrier, S. Kinetic investigation of photoiniferter-RAFT polymerization in continuous flow using inline NMR analysis. *Polym. Chem.* **2024**, *15*, 3166.

(5) Nwoko, T.; De Alwis Watuthanthrige, N.; Parnitzke, B.; Yehl, K.; Konkolewicz, D. Tuning the molecular weight distributions of

vinylketone-based polymers using RAFT photopolymerization and UV photodegradation. *Polym. Chem.* **2021**, *12* (46), 6761−6770.
(6) Ma, C.; Han, T.; Efstathiou, S.; Marathianos, A.; Houck, H. A.; Haddleton, D. M. Aggregation-Induced Emission Poly(meth)acrylates for Photopatterning via Wavelength-Dependent Visible-Light-Regulated Controlled Radical Polymerization in Batch and Flow Conditions. *Macromolecules* **2022**, *55* (22), 9908−9917.
(7) Bandyopadhyay, D.; Ji, Y.; Yee, D. W. Lights, chemistry, action plots: Rethinking photoresin design in additive manufacturing. *Matter* **2024**, *7* (8), 2745−2747.
(8) Walden, S. L.; Carroll, J. A.; Unterreiner, A.-N.; Barner-Kowollik, C. Photochemical Action Plots Reveal the Fundamental Mismatch Between Absorptivity and Photochemical Reactivity. *Adv. Sci.* **2024**, *11* (3), 2306014.
(9) Kalayci, K.; Frisch, H.; Truong, V. X.; Barner-Kowollik, C. Green light triggered [2 + 2] cycloaddition of halochromic styrylquinoxaline—controlling photoreactivity by pH. *Nat. Commun.* **2020**, *11* (1), 4193.
(10) Gauci, S. C.; Du Prez, F. E.; Holloway, J. O.; Houck, H. A.; Barner-Kowollik, C. The Power of Action Plots: Unveiling Reaction Selectivity of Light-Stabilized Dynamic Covalent Chemistry. *Angew. Chem., Int. Ed.* **2023**, *62*, e202310274.
(11) Feist, F.; Walden, S. L.; Alves, J.; Kunz, S. V.; Micallef, A. S.; Brock, A. J.; McMurtrie, J. C.; Weil, T.; Blinco, J. P.; Barner-Kowollik, C. Wavelength-Gated Photochemical Synthesis of Phenalene Diimides. *Angew. Chem., Int. Ed.* **2021**, *60* (18), 10402−10408.
(12) Kamm, P. W.; Blinco, J. P.; Unterreiner, A.-N.; Barner-Kowollik, C. Green-light induced cycloadditions. *Chem. Commun.* **2021**, *57* (33), 3991−3994.
(13) Michenfelder, R. T.; Pashley-Johnson, F.; Guschin, V.; Delafresnaye, L.; Truong, V. X.; Wagenknecht, H.-A.; Barner-Kowollik, C. Photochemical Action Plots Map Orthogonal Reactivity in Photochemical Release Systems. *Adv. Sci.* **2024**, *11* (29), 2402011.
(14) Carroll, J. A.; Pashley-Johnson, F.; Frisch, H.; Barner-Kowollik, C. Photochemical Action Plots Reveal Red-shifted Wavelength-dependent Photoproduct Distributions. *Chemistry − Eur. J.* **2024**, *30* (23), No. e202304174.
(15) Noon, A.; Hammoud, F.; Graff, B.; Hamieh, T.; Toufaily, J.; Morlet-Savary, F.; Schmitt, M.; Bui, T.-T.; Rico, A.; Goubard, F.; et al. Photoinitiation Mechanisms of Novel Phenothiazine-Based Oxime and Oxime Esters Acting as Visible Light Sensitive Type I and Multicomponent Photoinitiators. *Adv. Mater. Technol.* **2023**, *8* (16), 2300205.
(16) Ma, X.; Gu, R.; Yu, L.; Han, W.; Li, J.; Li, X.; Wang, T. Conjugated phenothiazine oxime esters as free radical photoinitiators. *Polym. Chem.* **2017**, *8* (39), 6134−6142.
(17) Liu, S.; Giacoletto, N.; Schmitt, M.; Nechab, M.; Graff, B.; Morlet-Savary, F.; Xiao, P.; Dumur, F.; Lalevée, J. Effect of Decarboxylation on the Photoinitiation Behavior of Nitrocarbazole-Based Oxime Esters. *Macromolecules* **2022**, *55* (7), 2475−2485.
(18) Gruendling, T.; Guilhaus, M.; Barner-Kowollik, C. Fast and Accurate Determination of Absolute Individual Molecular Weight Distributions from Mixtures of Polymers via Size Exclusion Chromatography−Electrospray Ionization Mass Spectrometry. *Macromolecules* **2009**, *42* (17), 6366−6374.
(19) Desport, J. S.; Frache, G.; Patiny, L. A web-based App for polymer mass spectrometry data interpretation. The case study of a pharmaceutical excipient. *Rapid Commun. Mass Spectrom.* **2020**, *34* (S2), No. e8652.
(20) Olaj, O. F.; Bitai, I.; Hinkelmann, F. The laser-flash-initiated polymerization as a tool of evaluating (individual) kinetic constants of free-radical polymerization, 2. The direct determination of the rate of constant of chain propagation. *Makromol. Chem.* **1987**, *188* (7), 1689−1702.
(21) Beuermann, S.; Buback, M.; Davis, T. P.; Gilbert, R. G.; Hutchinson, R. A.; Kajiwara, A.; Klumperman, B.; Russell, G. T. Critically evaluated rate coefficients for free-radical polymerization, 3. Propagation rate coefficients for alkyl methacrylates. *Macromol. Chem. Phys.* **2000**, *201* (12), 1355−1364.
(22) Beuermann, S.; Buback, M.; Davis, T. P.; Gilbert, R. G.; Hutchinson, R. A.; Olaj, O. F.; Russell, G. T.; Schweer, J.; van Herk, A. M. Critically evaluated rate coefficients for free-radical polymerization, 2.. Propagation rate coefficients for methyl methacrylate. *Macromol. Chem. Phys.* **1997**, *198* (5), 1545−1560.
(23) Hutchinson, R. A.; Beuermann, S. Critically evaluated propagation rate coefficients for radical polymerizations: acrylates and vinyl acetate in bulk (IUPAC Technical Report). *Pure Appl. Chem.* **2019**, *91* (11), 1883−1888.
(24) Lakowicz, J. R. *Principles of Fluorescence Spectroscopy*; Springer: 2006.
(25) Voll, D.; Neshchadin, D.; Hiltebrandt, K.; Gescheidt, G.; Barner-Kowollik, C. UV-Triggered End Group Conversion of Photo-Initiated Poly(methyl methacrylate). *Macromolecules* **2012**, *45* (15), 5850−5858.
(26) Thijssen, Q.; Carroll, J. A.; Feist, F.; Beil, A.; Grützmacher, H.; Wegener, M.; Van Vlierberghe, S.; Barner-Kowollik, C. Beyond absorption maxima: the impact of wavelength-resolved photochemistry on materials science. *Mater. Horiz.* **2024**, DOI: 10.1039/D4MH00976B.
(27) Sameshima, K.; Kawakami, T.; Sotome, H.; Fuki, M.; Kobori, Y.; Miyasaka, H. Dynamics and mechanism of radical formation in a highly sensitive oxime photoinitiator as revealed by time-resolved absorption and EPR measurements. *J. Photochem. Photobiol., A* **2023**, *437*, 114479.